INORGANIC CHEMISTRY
FRONTIERS

RESEARCH ARTICLE

View Article Online
View Journal | View Issue

Cite this: *Inorg. Chem. Front.*, 2018, **5**, 1800

Phase segregation enabled scandium fluoride–lanthanide fluoride Janus nanoparticles†

Pei-Zhi Zhang, Rui Liu, Ling-Dong Sun,* Hao Dong, Lin-Dong Li, Xiao-Yu Zheng, Ke Wu and Chun-Hua Yan *

Received 10th April 2018,
Accepted 18th May 2018

DOI: 10.1039/c8qi00328a

rsc.li/frontiers-inorganic

Janus particles, in which two distinct compositions are integrated, have attracted considerable interest for their potential multi-functionalities and synergistic effects. Although seed-mediated growth appears to be a suitable strategy that meets the stringent specifications for obtaining Janus particles, it is inapplicable to guide the growth of two crystalline components with different crystal structures. Herein, the formation of Janus particles *via* phase segregation is proposed. As proof-of-concept, promising photon conversion materials, ScF_3 and lanthanide (Ln) fluorides, with great differences in structure, were chosen to build a series of Janus particles. Interestingly, using heavy (Lu, Yb, Dy and Tb) and light (Pr, Nd, Sm, Eu and Gd) lanthanides, ScF_3–$LiLnF_4$ and ScF_3–LnF_3 were formed, respectively. Time-dependent reaction studies indicate that phase segregation paves the way for the formation of these Janus nanoparticles (NPs), and this speculation is further confirmed by *in situ* transmission electron microscopy observations. These investigations provide new insights for the synthesis of heterostructured materials.

Introduction

Heterostructured nanoparticles (NPs) with desired functionalities have become a hot topic in nanoscience.[1,2] As the simplest of heterostructures, Janus structure and core/shell (C/S) structure have received extensive attention. Similar crystal structures and closely matched lattice parameters (discrepancy of usually <3%)[3,4] between core and shell components are preferred for C/S structure fabrication, thus greatly narrowing the selection of core or shell materials. In contrast, Janus structure connects two components asymmetrically, partially relaxing the lattice match requirement.[5] Owing to the exposure of two different surfaces,[6] Janus structures can also act as platforms for flexible surface functionalization[7] or various chemical reaction possibilities.[8] Moreover, integrating different materials can give rise to emergent properties and even synergistic effects,[9] as reported for Au/CeO_2 Janus structures, for which good catalytic performance was obtained due to the hetero-interface electron transfer.[10] In light of these advantages, Janus structures have been studied for applications in heterogeneous catalysis,[11] magnetics,[12] electrochemical detection,[13] and even nanomachines,[14] bioimaging,[15] and theranostics.[16,17] Typically Janus structures are synthesized using the seed-growth method,[18,19] namely anisotropic nucleation on crystalline seeds,[20] which limits the integration of two building blocks with different crystal structures or/and guest building block with mismatched facets.[21,22] Hence, an effective alternate synthetic route to seed-growth method should be developed.

Lanthanide (Ln) fluorides are promising photon conversion materials due to their narrow-band emission, high photostability and long luminescent lifetimes.[23,24] Heterostructured lanthanide fluorides have attracted research interests in energy transfer,[25,26] bioimaging,[27] theranostics,[11] multicolor emission,[28] and multiplexed detection.[29] However, Janus structures are rarely studied for these applications because of the heterogeneous isomorphism of lanthanide fluorides.[30] On account of the lanthanide contraction and the varied structures that come from vacancies, the synthesis for lanthanide Janus particles has not been developed so far. Compared with lanthanide elements, scandium features a distinct electronic configuration and a smaller radius; thus, Sc^{3+}-based nanomaterials endow lanthanide ions with unique optical performances.[31] Moreover, cubic ScF_3 has different crystal structure from that of lanthanide fluorides, including $LiLnF_4$ and LnF_3 (Tables S1 and S2 of ESI†). Therefore, it is desirable to investigate the strategy for preparing Janus particles with scandium fluoride and lanthanide fluorides as building blocks and the effect on their intrinsic properties.

Herein, a phase segregation protocol is proposed to fabricate a series of scandium fluoride–lanthanide fluoride

Beijing National Laboratory for Molecular Sciences, State Key Laboratory of Rare Earth Materials Chemistry and Applications, PKU-HKU Joint Laboratory in Rare Earth Materials and Bioinorganic Chemistry, College of Chemistry and Molecular Engineering, Peking University, Beijing 100871, China. E-mail: sun@pku.edu.cn, yan@pku.edu.cn; Fax: +86-10-62754179; Tel: +86-10-62754179

†Electronic supplementary information (ESI) available: Experimental methods and supporting figures. See DOI: 10.1039/c8qi00328a

Janus structures. Interestingly, ScF_3–$LiLnF_4$ and ScF_3–LnF_3 were formed using heavy (Lu, Yb, Dy and Tb) and light (Pr, Nd, Sm, Eu and Gd) lanthanides, respectively. As demonstrated in ScF_3–$LiYbF_4$ NPs, a phase segregation process is crucial for the formation of Janus particles as confirmed *via in situ* TEM observations. These findings indicate that this protocol could be a valuable supplement for multiple heterostructures.

Results and discussion

The Janus structure NPs with a ScF_3–$LiYbF_4$ hetero-interface were synthesized by a modified thermal decomposition method.[32] As shown in Fig. 1a and b, these highly uniform Janus NPs are composed of a hemisphere with a diameter of 19.3 ± 1.1 nm and a truncated cube with a side length of 23.4 ± 2.3 nm. High-angle annular dark field-scanning transmission electron microscopy (HAADF-STEM) image shows a distinct contrast (Fig. 1c) and reveals the heterogeneous mass distributions between these two regions. STEM-energy dispersive X-ray spectroscopy (EDS) line scan result (Fig. 1d) and elemental mapping (Fig. 1e) further verify that scandium is mostly present in the light grey truncated cubic region and ytterbium is dominant in the bright hemi-spherical area. The X-ray diffraction (XRD) patterns (Fig. 1f) illustrate that these NPs consist of cubic ScF_3 (ICDD: 00-046-1243) and tetragonal $LiYbF_4$ (ICDD: 01-071-1211). Collectively, these results indicate that the truncated cubic region corresponds to cubic ScF_3 and the hemi-spherical area corresponds to tetragonal $LiYbF_4$. These results agree well with legible lattice distances measured in the high resolution TEM (HRTEM) images (Fig. 1g). In the light grey truncated cubic region, the lattice distance of 0.41 nm can be measured, corresponding to the {100} planes of cubic ScF_3. Moreover, the lattice distance of 0.46 nm measured in the hemispherical area can be indexed to the {101} planes of tetragonal $LiYbF_4$.

Despite distinct crystal structures of ScF_3 and $LiYbF_4$, the synthesis of ScF_3–$LiYbF_4$ Janus NPs was achieved by a one pot reaction. To investigate the formation mechanism of these Janus NPs, aliquots of reaction mixtures were taken at different reaction times at 320 °C. Representative HAADF-STEM and HRTEM images are shown in Fig. 2, highlighting the typical changes in the shape and structure of the NPs.

At 8 min, the NPs are quasi-spheres with diameters of 2–8 nm (Fig. 2a). Inductively coupled plasma-atomic emission spectroscopy (ICP-AES) suggests that these NPs contain Yb^{3+}/Sc^{3+}/Li^+ with an average ratio of 0.10/0.24/1.00 (Table S3 of ESI†). However, it is difficult to identify their structure due to their poor crystallization (Fig. 2b and Fig. S1 red line†). At 10 min, they developed into composite nanoparticles (Fig. 2c) with similar elemental distribution tendencies for ytterbium and scandium (Fig. S2†). Significantly, the HRTEM image (Fig. 2d) illustrates that these NPs are composed of multiple separated crystal domains. The blue-stained central part is assigned to be cubic ScF_3 and the surrounding parts stained by yellow are likely to be intermediates. The three sets of lattice fringes obtained in the yellow parts and the corresponding diffraction (Fig. S1 orange line†) cannot be correlated with any Sc or/and Yb-based species. At 11.5 min, a small portion of products still retain polycrystalline domains and the yellow parts show lattice fringes of 0.31 nm (Fig. S3a and b†). Moreover, most of the NPs self-regulate *via* dissolution and recrystallization as well as ionic exchange into Janus NPs (Fig. 2e). A fraction of these Janus NPs have the same lattice fringes of 0.31 nm as observed for the polycrystalline NPs (Fig. 2f), implying the continuous evolution of the intermediates. At 13.5 min, almost all the particles evolve to Janus structures (Fig. 2g). Some can be identified as ScF_3–$LiYbF_4$ NPs (Fig. 2h), while the others continue structure evolution and coexist as intermediates and poorly crystallized portions (Fig. S4†).

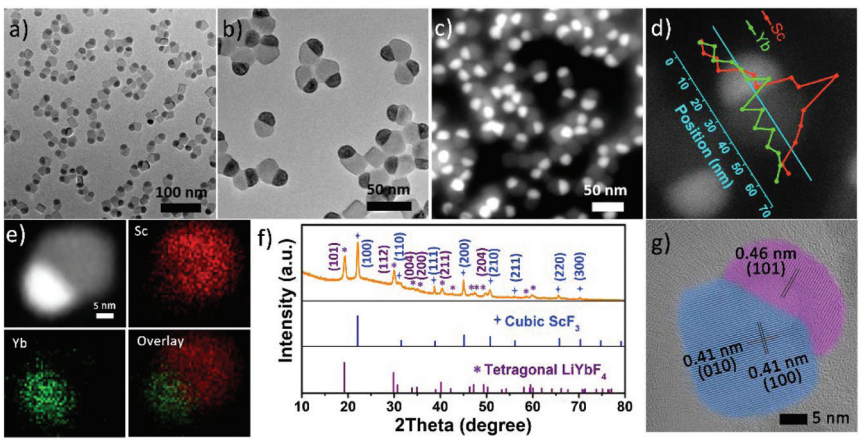

Fig. 1 (a, b) TEM images and (c) HAADF-STEM image of ScF_3–$LiYbF_4$ Janus NPs, (d) EDS line scan and (e) STEM-EDS elemental mapping of a single NP, which indicates the Sc and Yb elements are located in the cubic and hemispherical region, respectively. (f) XRD patterns of as-synthesized ScF_3–$LiYbF_4$ Janus NPs, and (g) HRTEM image of ScF_3–$LiYbF_4$ Janus NPs. Standard cubic ScF_3 (ICDD: 00-046-1243) and tetragonal $LiYbF_4$ (ICDD: 01-071-1211) patterns are also shown in (f).

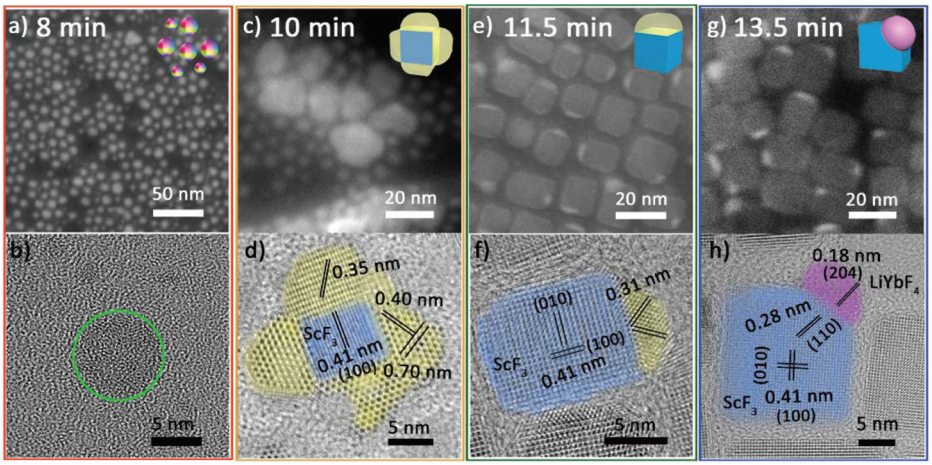

Fig. 2 TEM images of the temporal evolution of samples during the isothermal process. (a) and (b), (c) and (d), (e) and (f), and (g) and (h) correspond to HAADF-STEM image and HRTEM image of aliquots taken at 8 min, 10 min, 11.5 min and 13.5 min, respectively.

In order to elucidate the driving force for the transformation from the nucleation products to Janus NPs, the sample obtained at 8 min were separated from reaction solution and heated to 320 °C by an *in situ* heating holder loaded on a TEM. After 1 h, the NPs transform into Janus NPs (Fig. 3a), and the corresponding HRTEM image identifies them as ScF_3–$LiYbF_4$ (Fig. 3b) although they are not uniform in size. Without additional feeding of chemicals, the nucleation products still transform into Janus NPs *via in situ* heating, implying that heating-induced phase segregation is crucial for the formation of these Janus NPs.[33]

The importance of phase segregation was further confirmed by control experiments carried out using the seed-growth method. As shown in Fig. S5,† with ScF_3 NPs (Fig. S5a†) or lithium containing ScF_3 NPs (abbreviated as $ScF_3(Li^+)$, Fig. S5b†) as the starting seeds, isolated ScF_3 and $LiYbF_4$ NPs, rather than Janus NPs, or core/shell NPs appeared as the final products (Fig. S5c–f†) after adding the other precursors (Li^+ and Yb^{3+} or Yb^{3+} only). Compared with the one pot reaction, well-crystallized ScF_3 or $ScF_3(Li^+)$ with particular surfaces pose a large barrier for the nucleation of another component.

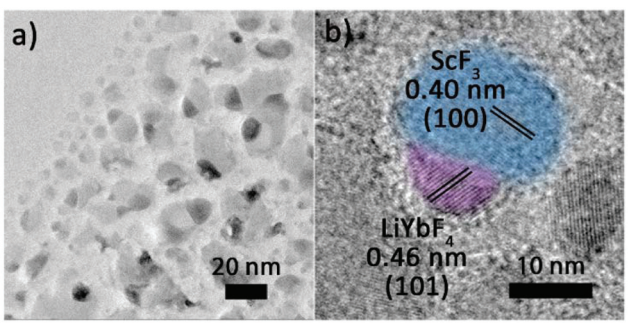

Fig. 3 *In situ* (a) TEM image and (b) HRTEM image of the final NPs after *in situ* heating the nucleation products (obtained at 8 min) at 320 °C for 1 h.

$LiYbF_4$ inclines to nucleate separately[34,35] to lower the total energy of the system.[36] In contrast, the phase separation induced Janus structure in the one pot reaction is unrestricted by the exposed facets of seeds, hence making it easier to form a hetero-interface.

For two building blocks having different crystal structures and large lattice mismatch, the phase segregation-based protocol provides an effective way to construct Janus structures. To understand the feasibility of the hetero-interface formed between lattice-mismatched structures, we further investigated the nature of the interface. Based on the hetero-interface details in HRTEM image (Fig. 2h), {204} planes of $LiYbF_4$ are parallel to the {110} planes of ScF_3. From the geometry of the crystal structures (Fig. S6a and S6b†), the distance between two F^- is 1.475 nm in the {204} planes of $LiYbF_4$, which is 1.5 times of that in ScF_3 {110} planes (0.982 nm). In addition, the interplanar spacing of {204} facets is 0.184 nm for $LiYbF_4$ (Fig. S6c†), while that of {110} planes for ScF_3 is 0.284 nm (Fig. S6d†). The facet mismatch of $|2d_{\{110\}} - 3d_{\{204\}}|/3d_{\{204\}}$ is 2.9%, *i.e.*, less than 5%. Moreover, this facet match can be revealed from the fast Fourier transformation (FFT) patterns of the overall ScF_3–$LiYbF_4$ Janus nanoparticle (Fig. S7a†), $LiYbF_4$ (Fig. S7b†) and ScF_3 (Fig. S7c†) domains. It can be seen that spots 1 and 2, which correspond to the {204} plane of $LiYbF_4$ and {110} plane of ScF_3, respectively, are aligned across the center. Collectively, these results indicate the well-matched {204} planes of $LiYbF_4$ and {110} planes of ScF_3.

Based on the abovementioned results, the formation process of the Janus nanostructure is illustrated in Scheme 1. The growth starts from homogeneous nucleation of mixed cation species with thermolysis of metal trifluoroacetates, and phase segregation causes further growth to form Janus NPs.[37] Throughout the process, phase segregation plays an important role in integrating two distinct crystals.

In addition to those of Yb^{3+}, Janus NPs with other heavy lanthanides, namely, Lu, Dy and Tb were also synthesized (Fig. 4a, Fig. S8a and b†) and identified as ScF_3–$LiLnF_4$

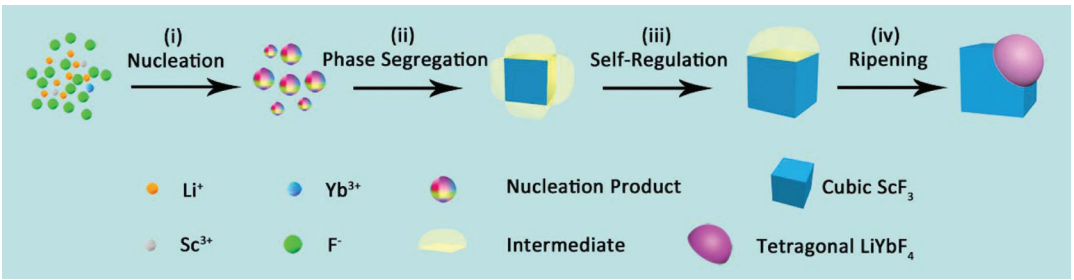

Scheme 1 The formation mechanism of ScF_3–$LiYbF_4$ Janus NPs.

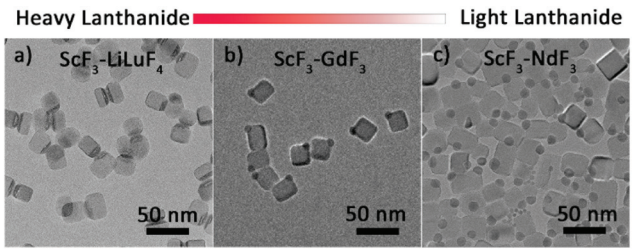

Fig. 4 The TEM images of TEM images of as-prepared scandium fluoride–lanthanide fluoride Janus NPs, lanthanide = Lu, Gd, and Nd.

(Fig. S9†). Interestingly, although the light lanthanides Pr, Nd, Sm, and Eu and the borderline lanthanide Gd do not favor the formation of tetragonal $LiLnF_4$,[38] Janus structures consisting cubic ScF_3 and hexagonal LnF_3 were still formed (Fig. 4b, c and Fig. S8c–e†), which was confirmed by XRD data (Fig. S10a–e†). The formation mechanism is similar to that of ScF_3–$LiYbF_4$ (Fig. S11†), as demonstrated in ScF_3–NdF_3. The above results indicate that the phase segregation protocol is applicable to Ln-based Janus NPs.

To study the optical performance of the Janus-structured NPs, 2%Er^{3+}/2%Ho^{3+}/0.5%Tm^{3+} doped ScF_3–$LiYbF_4$ Janus NPs were prepared (Fig. S12†) and the corresponding optical spectra were collected (Fig. S13†). Herein, Er^{3+} doped ScF_3–$LiYbF_4$ Janus NPs were analysed as a typical example, and a higher doping concentration of 6%, instead of the typical doping of 2%, was chosen to clearly identify the distribution of the dopant in a single ScF_3–$LiYbF_4$ NP. In the entire Janus NP, Er^{3+} and Yb^{3+} are mostly present in the $LiYbF_4$ portion (Fig. 5a and b). Under the 980 nm laser excitation, these NPs yield typical upconversion and near-infrared emissions of Er^{3+} (Fig. 5c) with peaks located at 410 nm ($^2H_{9/2} \rightarrow {}^4I_{15/2}$), 525 nm ($^2H_{11/2} \rightarrow I_{15/2}$), 545 nm ($^4S_{3/2} \rightarrow I_{15/2}$), 655 nm ($^4F_{9/2} \rightarrow {}^4I_{15/2}$)[39,40] and 1530 nm ($^4I_{13/2} \rightarrow {}^4I_{15/2}$).[41] Furthermore, these Janus NPs present a red-to-green ratio (R/G) of 1.32, which is higher than that of 2%Er^{3+} doped Janus NPs (Fig. S12a,† R/G = 0.84). This is probably attributed to the higher cross relaxation rate at an elevated content of Er^{3+}.

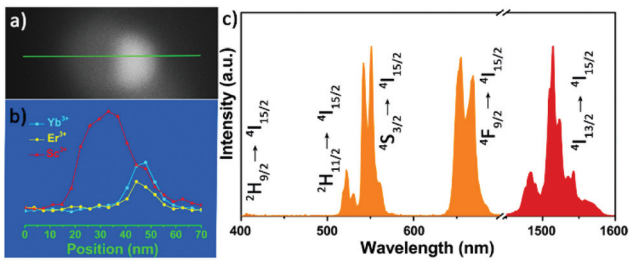

Fig. 5 (a) The HAADF-STEM image (b) EDS line scan of a single Er^{3+} (6%) doped ScF_3–$LiYbF_4$ Janus NP, and (c) normalized upconversion and near-infrared emission spectra of Er^{3+} (6%) doped ScF_3–$LiYbF_4$ Janus NPs. NPs are irradiated by 980 nm laser (24 W cm^{-2}).

Conclusions

A phase segregation-based protocol was presented to synthesize Janus particles consisting of two parts with different crystal structures. With this design, a series of scandium fluoride–lanthanide fluoride Janus NPs were synthesized for the first time. The formation of Janus NPs starts from homogeneous nucleation of mixed cation species, which undergoes phase segregation for the further growth towards scandium fluoride and lanthanide fluorides. Throughout the process, the phase segregation is the crucial step for the formation of Janus NPs. This synthetic method may provide new insights into the synthesis of heterostructures.

Conflicts of interest

There are no conflicts to declare.

Acknowledgements

This study was supported by NSFC (No. 21425101, 21371011, 21331001, 21590791) and MOST of China (2014CB643800, 2017YFA0205101).

Notes and references

1 P. D. Cozzoli and L. Manna, *Nat. Mater.*, 2005, **4**, 801–802.
2 T. Mokari, E. Rothenberg, I. Popov, R. Costi and U. Banin, *Science*, 2004, **304**, 1787–1790.

3 L. Carbone and P. D. Cozzoli, *Nano Today*, 2010, **5**, 449–493.
4 C. Tan, J. Chen, X.-J. Wu and H. Zhang, *Nat. Rev. Mater.*, 2018, **3**, 17089.
5 T. Chen, G. Chen, S. Xing, T. Wu and H. Chen, *Chem. Mater.*, 2010, **22**, 3826–3828.
6 J. M. Hodges, J. R. Morse, M. E. Williams and R. E. Schaak, *J. Am. Chem. Soc.*, 2015, **137**, 15493–15500.
7 I. Schick, S. Lorenz, D. Gehrig, A.-M. Schilmann, H. Bauer, M. Panthöfer, K. Fischer, D. Strand, F. Laquai and W. Tremel, *J. Am. Chem. Soc.*, 2014, **136**, 2473–2483.
8 F. Wang, G. M. Pauletti, J. Wang, J. Zhang, R. C. Ewing, Y. Wang and D. Shi, *Adv. Mater.*, 2013, **25**, 3485–3489.
9 Z. W. She, S. Liu, M. Low, S.-Y. Zhang, Z. Liu, A. Mlayah and M.-Y. Han, *Adv. Mater.*, 2012, **24**, 2310–2314.
10 Z.-X. Li, W. Xue, B.-T. Guan, F.-B. Shi, Z.-J. Shi, H. Jiang and C.-H. Yan, *Nanoscale*, 2013, **5**, 1213–1220.
11 C. George, A. Genovese, A. Casu, M. Prato, M. Povia, L. Manna and T. Montanari, *Nano Lett.*, 2013, **13**, 752–757.
12 A. Figuerola, A. Fiore, R. Di Corato, A. Falqui, C. Giannini, E. Micotti, A. Lascialfari, M. Corti, R. Cingolani, T. Pellegrino, P. D. Cozzoli and L. Manna, *J. Am. Chem. Soc.*, 2008, **130**, 1477–1487.
13 X. Sun, S. Guo, Y. Liu and S. Sun, *Nano Lett.*, 2012, **12**, 4859–4863.
14 W. Qin, T. Peng, Y. Gao, F. Wang, X. Hu, K. Wang, J. Shi, D. Li, J. Ren and C. Fan, *Angew. Chem., Int. Ed.*, 2017, **56**, 515–518.
15 J. Jiang, H. Gu, H. Shao and E. Devlin, *Adv. Mater.*, 2008, **20**, 4403–4407.
16 X. Li, L. Zhou, Y. Wei, A. M. Ei-Toni, F. Zhang and D. Zhao, *J. Am. Chem. Soc.*, 2014, **136**, 15086–15092.
17 Y. Li, Z. Di, J. Gao, P. Cheng, C. Di, G. Zhang, B. Liu, X. Shi, L.-D. Sun, L. Li and C.-H. Yan, *J. Am. Chem. Soc.*, 2017, **139**, 13804–13810.
18 T.-T. Zhuang, F.-J. Fa, M. Gong and S.-H. Yu, *Chem. Commun.*, 2012, **48**, 9762–9764.
19 A. A. Lutich, C. Mauser, E. D. Como, J. Huang, A. Vaneski, D. V. Talapin, A. L. Rogach and J. Feldmann, *Nano Lett.*, 2010, **10**, 4646–4650.
20 S. Liang, X.-L. Liu, Y.-Z. Yang, Y.-L. Wang, J.-H. Wang, Z.-J. Yang, L.-B. Wang, S.-F. Jia, X.-F. Yu, L. Zhou, J.-B. Wang, J. Zeng, Q.-Q. Wang and Z. Zhang, *Nano Lett.*, 2012, **12**, 5281–5286.
21 J. E. Prieto and I. Markov, *Surf. Sci.*, 2017, **664**, 172–184.
22 J. Zhang, Y. Tang, K. Lee and M. Ouyang, *Science*, 2010, **327**, 1634–1638.
23 H. Dong, L.-D. Sun, Y.-F. Wang, J. Ke, R. Si, J. Xiao, G.-M. Lyu, S. Shi and C.-H. Yan, *J. Am. Chem. Soc.*, 2015, **137**, 6569–6581.
24 G. Chen, H. Qiu, P. N. Prasad and X. Chen, *Chem. Rev.*, 2014, **114**, 5161–5214.
25 X. Chen, L. Jin, W. Kong, T. Sun, W. Zhang, X. Liu, J. Fan, S. F. Yu and F. Wang, *Nat. Commun.*, 2016, **7**, 10304.
26 Y. Liu, S. Zhou, Z. Zhuo, R. Li, Z. Chen, M. Hong and X. Chen, *Chem. Sci.*, 2016, **7**, 5013–5019.
27 X. Zhu, W. Feng, J. Chang, Y.-W. Tan, J. Li, M. Chen, Y. Sun and F. Li, *Nat. Commun.*, 2016, **7**, 10437.
28 R. Deng, F. Qin, R. Chen, W. Huang, M. Hong and X. Liu, *Nat. Nanotechnol.*, 2015, **10**, 237–242.
29 L. Hu, Y. Fan, L. Liu, X. Li, B. Zhao, R. Wang, P. Wang, A. M. El-Toni and F. Zhang, *Adv. Opt. Mater.*, 2017, 1700680.
30 D. Liu, X. Xu, Y. Du, X. Qin, Y. Zhang, C. Ma, S. Wen, W. Ren, E. M. Goldys, J. A. Piper, S. Dou, X. Liu and D. Jin, *Nat. Commun.*, 2016, **7**, 10254.
31 X. Teng, Y. Zhu, W. Wei, S. Wang, J. Huang, R. Naccache, W. Hu, A. I. Y. Tok, Y. Han, Q. Zhang, Q. Fan, W. Huang, J. A. Capobianco and L. Huang, *J. Am. Chem. Soc.*, 2012, **134**, 8340–8343.
32 H.-X. Mai, Y.-W. Zhang, R. Si, Z.-G. Yan, L.-D. Sun, L.-P. You and C.-H. Yan, *J. Am. Chem. Soc.*, 2006, **128**, 6426–6436.
33 S.-K. Han, C. Gu, M. Gong, Z.-M. Wang and S.-H. Yu, *Small*, 2013, **9**, 3765–3769.
34 H. Q. Ta, D. J. Perello, D. L. Duong, G. H. Han, S. Gorantla, V. L. Nguyen, A. Bachmatiuk, S. V. Rotkin, Y. H. Lee and M. H. Rümmeli, *Nano Lett.*, 2016, **16**, 6403–6410.
35 S. E. Habas, H. Lee, V. Radmilovic, G. A. Somorjai and P. Yang, *Nat. Mater.*, 2007, **6**, 692–697.
36 Y. Feng, J. He, H. Wang, Y. Y. Tay, H. Sun, L. Zhu and H. Chen, *J. Am. Chem. Soc.*, 2012, **134**, 2004–2007.
37 T. Mokari, C. G. Aztrum, ASAF Salant, E. Rabani and U. Banin, *Nat. Mater.*, 2005, **4**, 855–863.
38 Q.-S. Qin, P.-Z. Zhang, L.-D. Sun, S. Shi, N.-X. Chen, H. Dong, X.-Y. Zheng, L.-M. Li and C.-H. Yan, *Nanoscale*, 2017, **9**, 4660–4664.
39 Q. Liu, Y. Sun, T. Yang, W. Feng, C. Li and F. Li, *J. Am. Chem. Soc.*, 2011, **133**, 17122–17125.
40 N. J. Greybush, M. Saboktakin, X. Ye, C. D. Giovampaola, S. J. Oh, N. E. Berry, N. Engheta, C. B. Murray and C. R. Kagan, *ACS Nano*, 2014, **8**, 9482–9491.
41 Y. Zhong, Z. Ma, S. Zhu, J. Yue, M. Zhang, A. L. Antaris, J. Yuan, R. Cui, H. Wan, Y. Zhou, W. Wang, N. F. Huang, J. Luo, Z. Hu and H. Dai, *Nat. Commun.*, 2017, **8**, 737.

